*Clean Energy*, 2023, Vol. 7, No. 5, 1058–1068
https://doi.org/10.1093/ce/zkad046
Advance access publication 26 September 2023
**Research Article**

# Effects of magnet shapes on total harmonic distortion and cogging torque in a permanent magnet synchronous generator for wind turbines

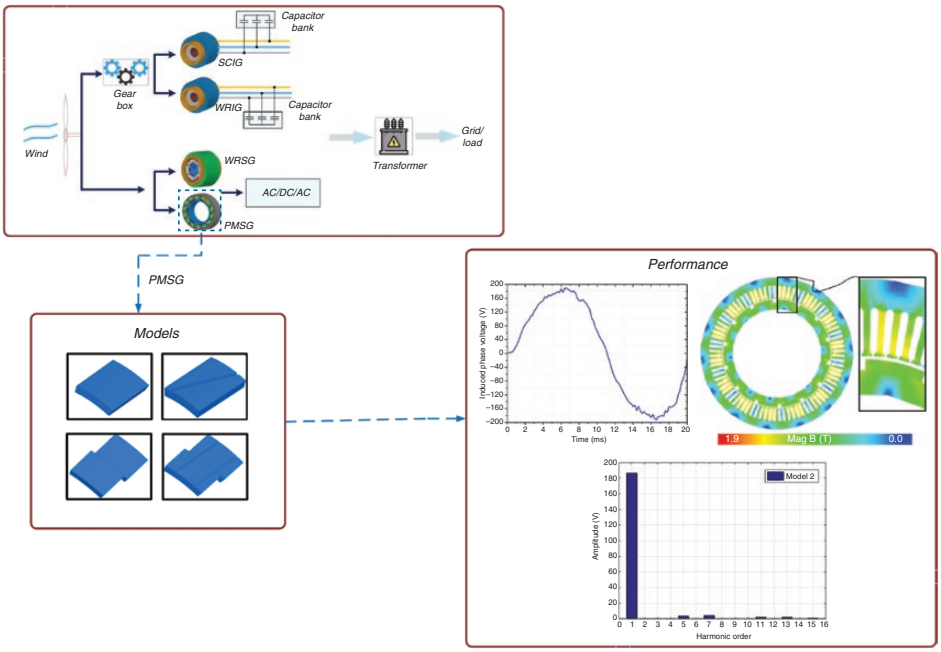
Erol Kurt[1] and Adem Dalcalı[2,3,*]

[1]Gazi University, Department of Electrical and Electronics Engineering, Technology Faculty, Ankara, Turkey
[2]Bandırma Onyedi Eylül University, Department of Electrical and Electronics Engineering, Faculty of Engineering and Natural Sciences, Bandırma, Balıkesir, Turkey
[3]National Research University, TIIAME, 100000, Tashkent, Uzbekistan
[*]Corresponding author. E-mail: adalcali@bandirma.edu.tr

## Abstract

This paper explores and theoretically reports the effects of different magnet structures on the cogging torque and the total harmonic distortion of the output waveforms from a permanent magnet generator. The generator is a radial flux machine and four different structures are considered for the magnet arrangement in the rotor component and modelled in the Ansys/Maxwell electromagnetic simulation program. This three-phase machine exhibits different behaviours towards various magnet structures, i.e. rectangular, inclined slotted rectangular, skewed double rectangular and inclined slotted skewed double rectangular, respectively. It has been proven by finite element analysis and Fourier analysis that both the cogging and total harmonic distortion values vary significantly for all models. The cogging torque values change in the range of 89.95 to 436.75 mNm and the lowest cogging torque is measured for the inclined slotted skewed double rectangular magnet geometry, while the conventional rectangular magnet geometry yields the worst value with 436.75 mNm. Furthermore, the total harmonic distortion values varies between 1.63 and 3.55 for different magnetic orientations. While the worst total harmonic distortion value is obtained from the inclined slotted rectangular magnet, the best total harmonic distortion is acquired from the skewed double rectangular magnet. All these results will provide scientists and engineers with important information in order to obtain more efficient machines.

## Graphical Abstract




**Keywords:** renewable energy; wind power; finite element method; synchronous generator; wind turbines

**Received:** 30 March 2023. **Accepted:** 13 June 2023
© The Author(s) 2023. Published by Oxford University Press on behalf of National Institute of Clean-and-Low-Carbon Energy
This is an Open Access article distributed under the terms of the Creative Commons Attribution-NonCommercial License (https://creativecommons.org/licenses/by-nc/4.0/), which permits non-commercial re-use, distribution, and reproduction in any medium, provided the original work is properly cited. For commercial re-use, please contact journals.permissions@oup.com

Downloaded from https://academic.oup.com/ce/article/7/5/1058/7283059 by ANKOS Consortium (UK - ANB Free Trial Account) user on 13 November 2023

## Introduction

Global energy consumption increases depending on the requirements that arise from population growth and industrial development. It is obvious that energy availability and sources of energy are not sustainable in the long term because fossil fuel reserves will expire in the near future and may even cause environmental damage during energy production worldwide [1]. At the same time, the popularity of low-cost, local and environmentally friendly renewable energy sources increases with each passing day. Wind energy, one of the renewable energy sources, plays an important role in ensuring energy reliability, reducing foreign dependence on energy and solving environmental problems, especially in countries with potential for wind energy [2]. This also improves motivation for designing and producing the new and efficient energy conversion mechanisms, especially generators, energy harvesters, converters and other power electronic components [3, 4].

The generators used in wind turbines are among the most important components of the system [5, 6]. Direct current (DC) generators, asynchronous generators, switched reluctance generators and synchronous generators are used in turbines. The DC generators need frequent maintenance due to the brush and collector. The asynchronous generators are inexpensive and have a robust structure. However, especially high pole applications are limited and have relatively low efficiency. The switched reluctance generators have acoustic noise and high torque fluctuations. It is possible to produce synchronous generators as rotor winding or permanent magnet (PM) synchronous generators. The absence of a brush assembly in permanent magnet synchronous generators (PMSGs) reduces the need for maintenance [7–9]. Moreover, rare-earth magnets made from NdFeB have provided new horizons on the way to having efficient, high-energy-density machines. As stated in the literature, PM machines can provide higher torque with lower weight than asynchronous and switched reluctance machines [10, 11]. It is possible to transfer the electrical energy generated in PM generators to the system or load by arranging it through power electronic components. The dynamic performance of the generator is improved and continuous power generation is facilitated in a wide speed range with the use of power electronic elements and magnets in the rotor. These advantages are increasingly used in PMSGs in renewable-energy applications [12, 13]. Furthermore, the rare-earth metals neodymium and dysprosium are needed to produce NdFeB-type magnets. Using these metals causes a constant need for raw materials, which can lead to supply problems and price fluctuations [8, 14, 15].

The generator performance is directly correlated with the material used and its physical structure. The structure of the stator slot, its dimensions and magnet geometry can improve the performance of the generator [16]. Some studies have been conducted in the literature on the magnet optimization of the PMSGs using numerical and finite element methods (FEM) [17–19]. In general, they have focused on optimizing the cogging torque (CT) [15, 20]. The CT is the interaction between the magnets and the stator teeth in PM machines. The CT causes torque fluctuation in the machine. This leads to mechanical vibrations and acoustic noise, which shortens the service life of the machine [21, 22]. In the study that examined the effects of magnet thickness, its material and pole-arc-to-pole-pitch ratio, the generator efficiency and CT were improved. Compared with the reference model, the CT decreased, while the efficiency and air gap flux density increased [23]. Another study proposed a bridge spoke-type PMSG as an alternative to a surface-mounted structure. Higher line voltage and lower CT were obtained from the proposed structure [24]. The study, in which the magnet length and radius were determined as variables, examined the PMSG designs that provided maximum efficiency at a minimum weight. Compared with the reference design, the decrease in efficiency and weight was provided with the change in the determined parameters [25]. Likewise, the magnet structure is effective in machines with axial-flux magnets. Amin *et al.* investigated the impact of trapezoidal, skewed, triangular and rounded-triangular magnets on the generator performance in their study. The analyses determined that the triangular structure provided high output power, while the rounded-triangular structure reduced this power [26]. The effect of CT in different electrical machines was investigated and reduction was attempted. As a different structure, the CT was optimized in the flux-switching PM machine. In the study, an arc-shaped triangular magnet structure was proposed. The CT decreased due to the effective air gap provided by the proposed magnet structure [27]. A new rotor structure was suggested to reduce the CT of the axial-flux internal rotor PM machine. At the first stage, a sinusoidal magnet structure was proposed. Second, the magnet overhang technique was employed to improve the performance of the machine. The proposed models were analysed by using 3D FEM. The CT was reduced by 46.68% in the first stage and by 69.34% in the second stage compared with the conventional structure [28]. In another study carried out on the magnet section, the structure with a pentagonal magnet was examined on the axial-flux-type PMSG. With the proposed magnet structure, low cogging and high output torque and efficiency were acquired compared with the classical structure [29]. In the study performed on the stator section, a new method based on shaping the stator tooth tips with sinusoidal profiles was suggested. The amplitudes and phase shifts of the sinusoidal profiles were determined by using a genetic algorithm and an optimization method based on artificial neural networks. The proposed method was examined on machines with different stator cores and an improvement of >80% was achieved [30]. To improve the CT, the effect of the dimensions of the rotor teeth and the change in the air gap between the stator and the rotor were investigated in the study carried out on the rotor section of the DC excited flux-switching machine motor. In the analyses, rounding the corners of the rotor teeth reduced the CT [31]. In another study conducted on the rotor section, optimization was carried out by changing the geometry of the rotor lamination package of the interior PM synchronous motor. Nine machine models were created with different rotor lamination angles and the angle value at which the CT was at the minimum was determined [32]. In general, the studies focused on the CT. However, their performance and total harmonic distortions at different loads and speeds were not detailed.

The present study examined 2.5-kW rated power for the PMSG. To this end, different magnetic surface-mounted PMSGs, which are used in wind turbines, were designed and simulated. Each simulation procedure includes the analysis based on magnetostatic and magnetodynamic manners. Although the validity of the designs was proved in finite element analyses, time-dependent electromagnetic solutions revealed phase voltage waveforms and cogging torques. Furthermore, the total harmonic distortion (THD) was analysed from the resulting waveforms. The graphical method, harmonic components and angles of voltages were used, and the THDs in percentages were subtracted from the patterns.

This paper is organized as follows. Section 1 introduces the proposed designs with the required physical parameters. The next section presents the main findings on CT and THD. A

Downloaded from https://academic.oup.com/ce/article/7/5/1058/7283059 by ANKOS Consortium (UK - ANB Free Trial Account) user on 13 November 2023

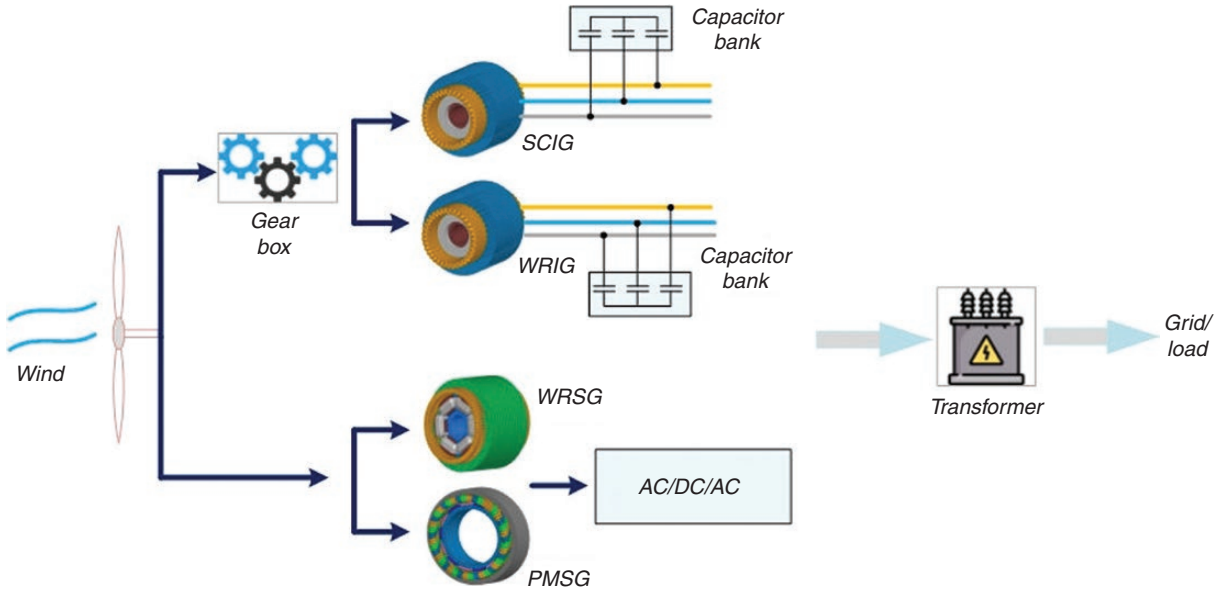



**Fig 1:** Wind turbine generator systems.

**Table 1:** Design parameters of the generator [37]

| Parameter | Value | Unit | Parameter | Value | Unit |
|---|---|---|---|---|---|
| Rated power | 2500 | W | Pole number | 14 | – |
| Frequency | 50 | Hz | Number of slots | 84 | – |
| Power factor | 0.95 | – | Permanent magnet material | N35 | – |
| Stator outer diameter | 280 | mm | Stator-rotor material | M19 | – |
| Length of stator | 54 | mm | Stator slot fill factor | 68.4 | % |

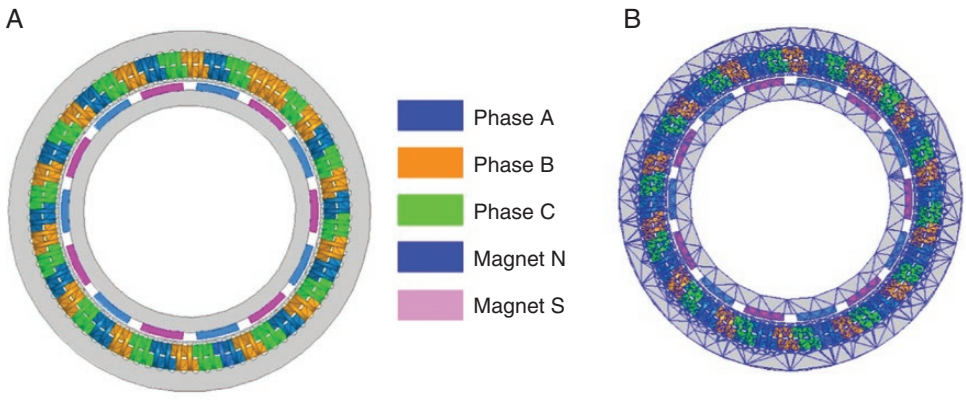



**Fig. 2:** Model of initial designed generator. (a) 3D version; (b) meshed version.

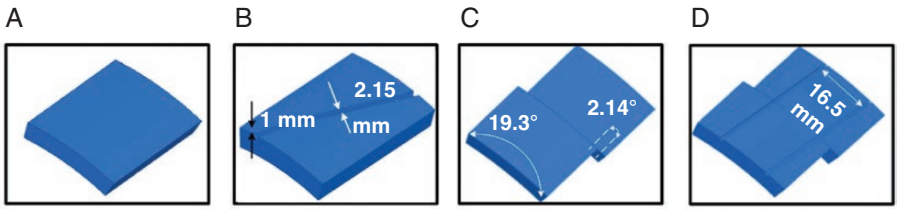



**Fig. 3:** Design types. (a) Rectangular (R), (b) inclined slotted rectangular (ISR), (c) skewed double rectangular (SDR) and (d) inclined slotted skewed double rectangular (ISSDR), respectively.

Downloaded from https://academic.oup.com/ce/article/7/5/1058/7283059 by ANKOS Consortium (UK - ANB Free Trial Account) user on 13 November 2023

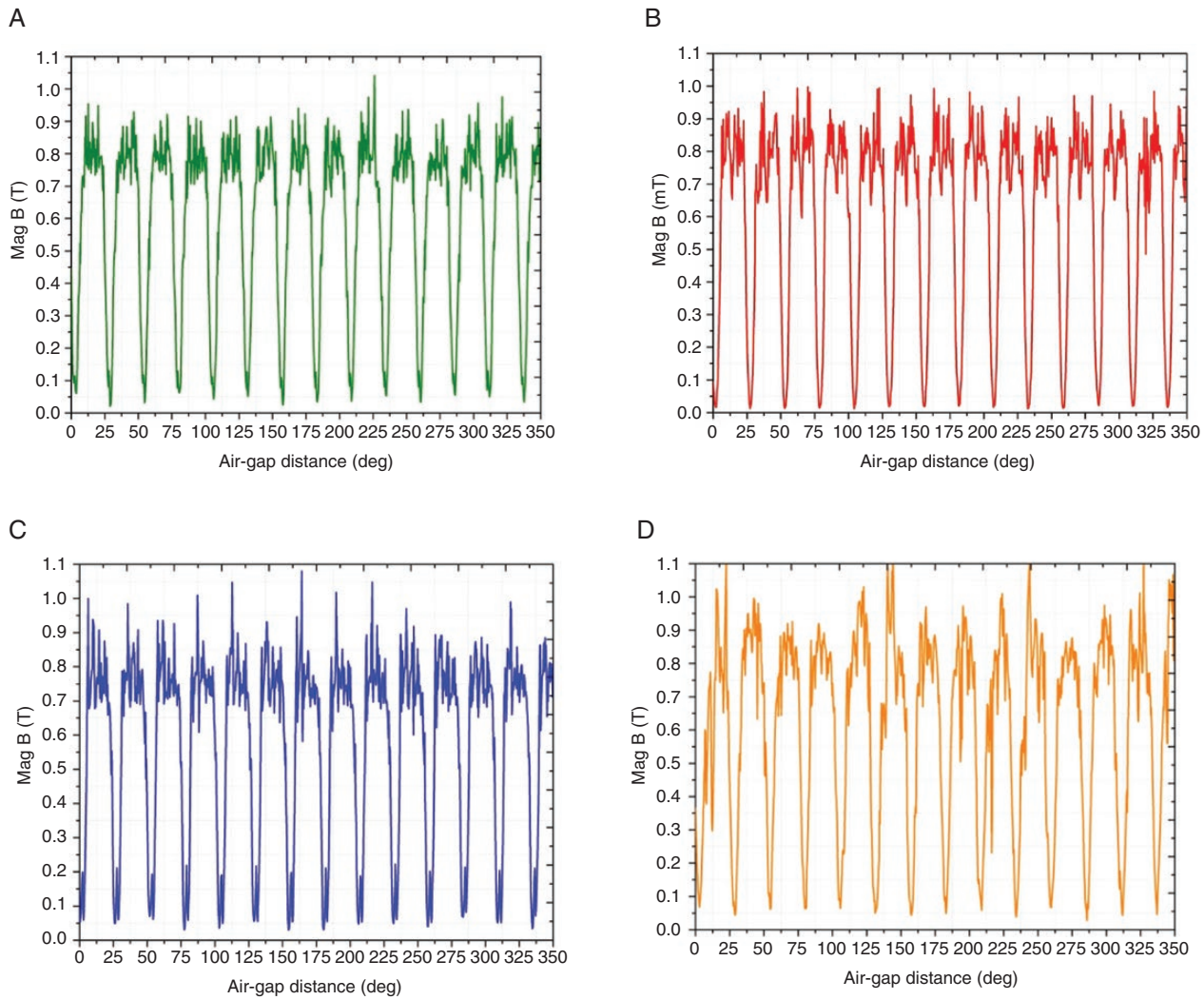



**Fig. 4:** The flux densities at the air gaps of (a) Design 1, (b) Design 2, (c) Design 3 and (d) Design 4, respectively at $\omega = 428.5$ rpm.

comprehensive discussion is also provided in this section. Finally, the concluding remarks are reported in the conclusion section.

## 1 Specification of designed PM generator

Many different types of generators are used in wind turbines. There are squirrel-cage induction generators and wound-rotor induction generators used with gearboxes in wind turbines. Wound-rotor synchronous generators and PMSGs do not require a gear box and are also used in turbines. Wind turbine systems are presented in Fig. 1.

PMSGs have high-efficiency and high-power-density characteristics. PM machines do not need a gear system and are often preferred, especially for low-speed and variable-speed applications. In these machines, magnets can be placed inside the rotor or on its surface. The interior structure is suitable for high-speed applications. However, in this structure, the effective air gap is reduced, which increases the armature reaction. There is an effective air gap in the surface-mounted structure [33].

The generator, which is the subject of the current study, is a 2.5-kW-powered three-phase surface-mounted PM machine with a direct drive and an inner rotor. This type of generator is frequently used in wind turbines to convert mechanical rotation energy into electricity, as it does not require any complicated gear systems [34–36]. Table 1 contains the design parameters.

PM materials can be classified mainly as alnico, ceramic and rare-earth magnets. The magnetization properties of ceramic magnets are lower than those of rare-earth element magnets. NdFeB-type magnets have high magnetic flux density ($B$) and the maximum magnetic energy is obtained by multiplying the flux density $B_{max}$ and the field strength $H_{max}$ [38]. Therefore, this type of magnet is widely used in different applications, such as the automotive industry, wind turbines and micro-electro-mechanical system applications requiring high power and torque density [39–41]. Fig. 2 shows a 3D model and the initial design of the generator with detailed mesh structure.

In this study, we examine the generator model with four different magnet structures, whose performance has previously been examined in [37], which was taken as a reference. Fig. 3 shows the rotor and magnet models of generators.

The design of electrical machines includes the solution of many complex problems, such as thermal, material and mechanical problems. In electrical machines, the magnet geometry, magnet orientation and material affect the machine performance. It is possible to enhance performance by skewing or splitting permanent magnets on the axial line. Design 1, abbreviated with R (rectangular), as a genuine and traditional structure, has magnets with N–S–N–S

Downloaded from https://academic.oup.com/ce/article/7/5/1058/7283059 by ANKOS Consortium (UK - ANB Free Trial Account) user on 13 November 2023

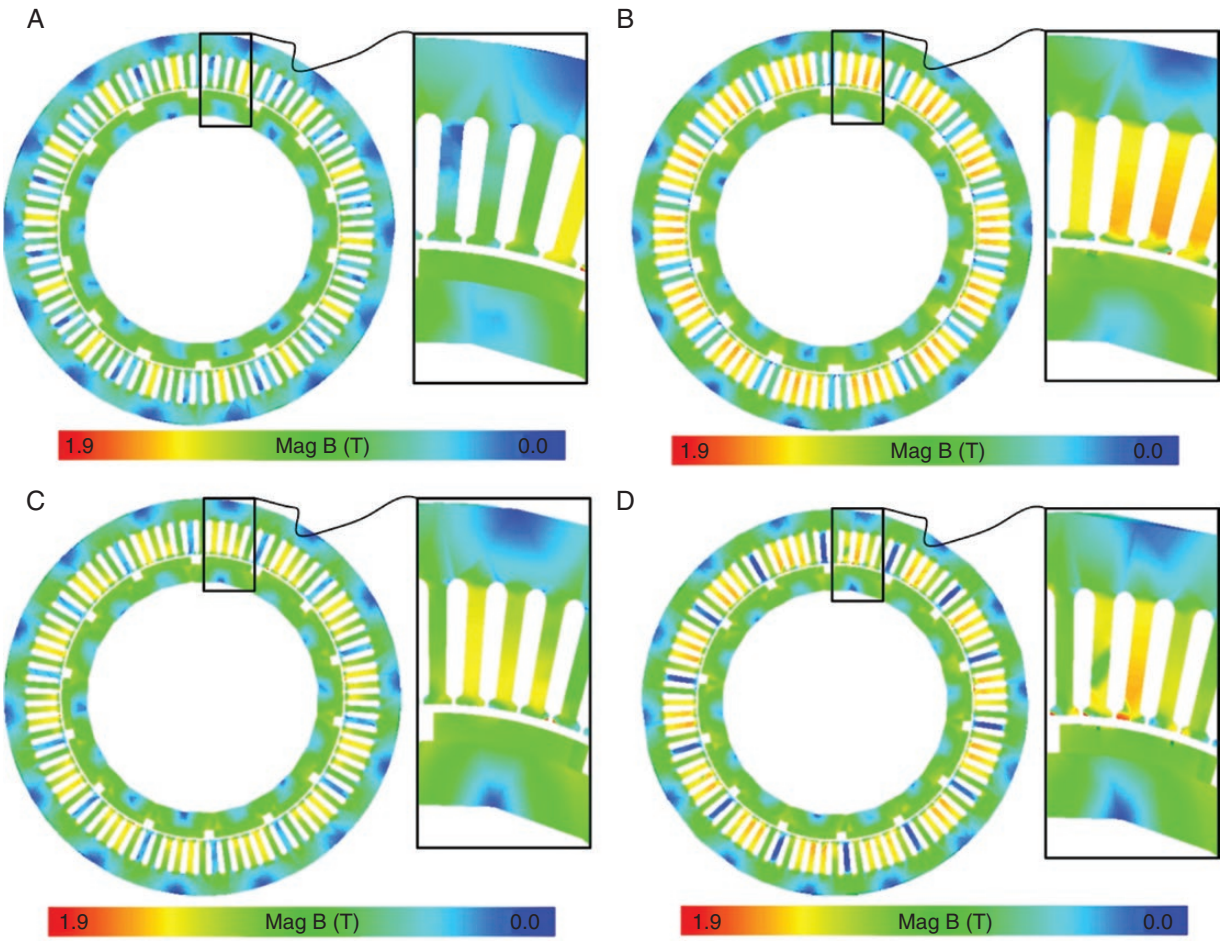



**Fig. 5:** The magnetic flux distribution in the core of (a) Design 1, (b) Design 2, (c) Design 3 and (d) Design 4, respectively, at ω = 428.5 rpm.

orientation without any slot or skewing. In Design 2 (inclined slotted rectangular (ISR)), a slot shown in Fig. 3b is opened on the magnet part by facing the stator surface. The slot is 1 mm in depth and 2.15 mm in thickness. In Design 3 (skewed double rectangular (SDR)), the magnet is divided into two equal parts. The last design, Design 4 (inclined slotted skewed double rectangular (ISSDR)), is obtained by opening two slots in the magnet. The mechanical magnitude of the angle of curvature of the magnet parts in the structures given in Designs 3 and 4 can be calculated as shown in Equation (1) [42]:

$$\theta = \frac{360}{n \times N_c \times S} \quad (1)$$

where $n$ defines the number of parts, $S$ represents the number of slots and $N_c$ demonstrates the period of the CT, calculated by using Equation (2):

$$N_c = \frac{2P}{HCF\ (2P,\ S)} \quad (2)$$

where $HCF$ represents the highest common factor and $2P$ the number of poles. The inclination angle for the generator designed according to Equations (1) and (2) is 2.14°.

## 2 Results and discussion

The magnetostatic analyses performed in the study were carried out using FEM. This method involves an approximate analysis of quantities that are continuous in a certain region and can be expressed by partial differential equations. The required quantities can be obtained by solving a set of linear equations, which are divided into a finite number of small regions and have as many equations as the number of nodes. FEM can be used to obtain performance values such as core losses, voltage–current waveforms, magnetic flux distributions, output power and efficiency [27].

### 2.1 Analysis of magnetic flux densities by FEM

Electromagnetic simulations proved the average flux densities of 0.607 T in the air gap of each design, as seen in Fig. 4a–d. The best magnetostatic performance was obtained from Design 4. However, we expect that a high-flux-density machine will suffer in terms of the CT, in parallel with the literature. Therefore, it is necessary to optimize the air gap by considering various scenarios such as slotting, skewing, etc. [37, 43].

According to the electromagnetic analyses conducted in line with the FEM, the sample magnetic fluxes ($\varphi$) were picked up in Fig. 5a–d at a speed of 428.5 rpm.

It is remarkable that the amplitudes of the magnetic fluxes do not change at a speed, while the period of the waveforms only changes at the generator speed in parallel with Faraday's law of induction.

### 2.2 Analysis of CT by FEM

The mathematical expression for the CT is a function of the air gap flux and the rotor position is expressed in Equation (3) [37, 44]:

Downloaded from https://academic.oup.com/ce/article/7/5/1058/7283059 by ANKOS Consortium (UK - ANB Free Trial Account) user on 13 November 2023

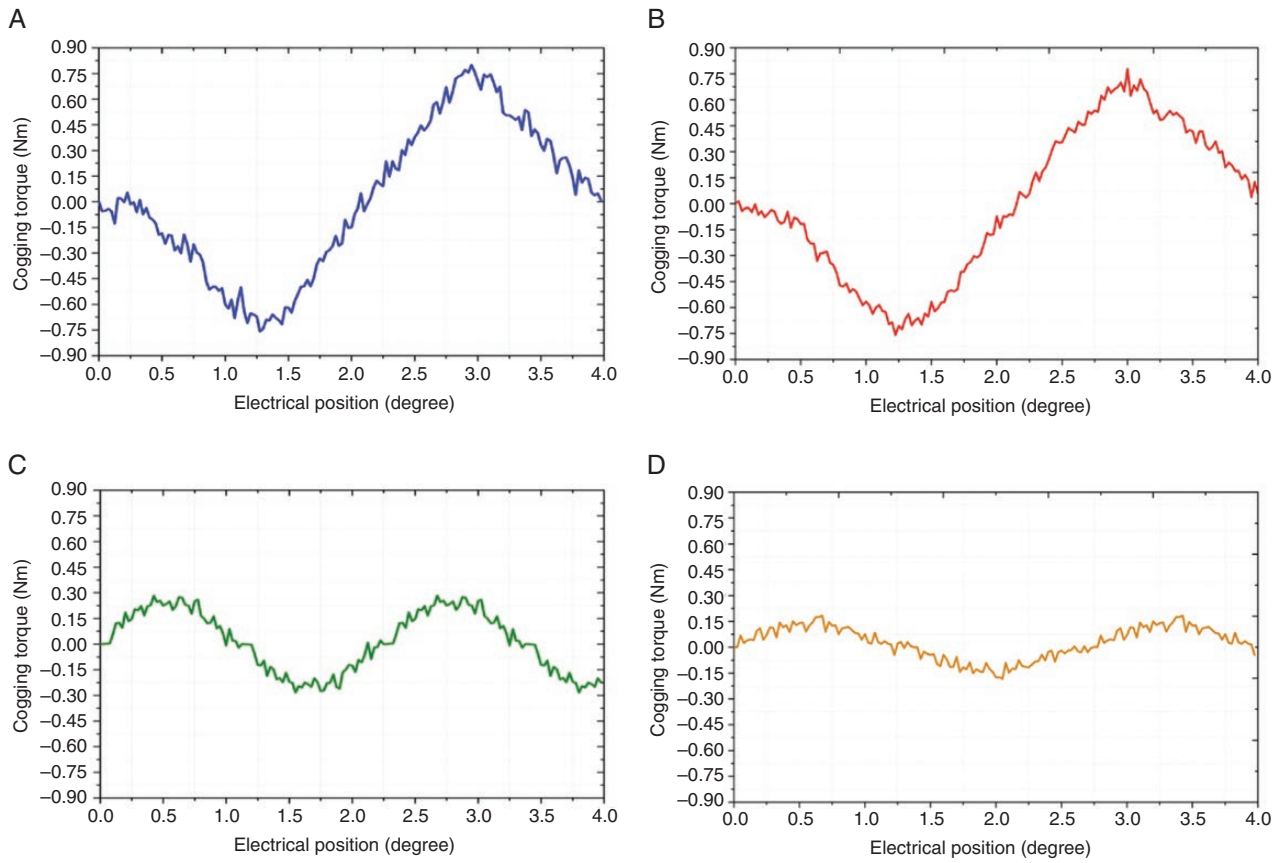



**Fig. 6:** Variation in cogging torques according to the electrical position of the rotor. (a) Design 1, (b) Design 2, (c) Design 3 and (d) Design 4, respectively.

**Table 2:** Rated powers and cogging torque of designs

| Design | Output power (W) | Cogging torque (mNm) |
|---|---|---|
| Design 1 (R) | 2500 | 436.75 |
| Design 2 (ISR) | 2462 | 434.58 |
| Design 3 (SDR) | 2455 | 159.60 |
| Design 4 (ISSDR) | 2431 | 89.95 |

$$T_{cog} = \frac{1}{2}\varphi_{air}^2 \frac{d\Re}{d\theta} \tag{3}$$

where $\varphi_{air}$ denotes the air gap flux, $\theta$ depicts the rotor position and $\Re$ represents the air gap reluctance. As seen in Equation (3), the CT is affected by the change in air gap reluctance. Since the air gap of the generator changes periodically, the CT will also change periodically and can be expressed as a Fourier series, as seen in Equation (4):

$$T_{cog} = \sum_{k=1}^{\infty} T_{mk} \sin(mk\theta) \tag{4}$$

where $T_{mk}$ represents the Fourier coefficient and $m$ defines the smallest multiple of the pole and slot number. Following the electromagnetic simulations, we also formed the CT values, as shown in Fig. 6a–d.

According to the output performances of the designs, both rated powers and CT values are summarized in Table 2. While Design 1 yields the highest power with 2.5 kW, the powers of Designs 2, 3 and 4 decreased to 2.46, 2.45 and 2.43, respectively. This only coincides with a 2.76% maximum decrease in the other designs. Such a low decrease in power does not give any overall side effects when the THD and CT are taken into account in the following part of the study.

## 2.3 Analysis of THD by using Fourier analysis

In power systems, it is desirable that electrical energy is continuous and of high quality. Harmonics are full multiples of the fundamental frequency in energy systems, causing distortions in the main voltage and load current waveforms. The presence of harmonic components causes a distortion in the waveform. These distorted waveforms can be analysed by using a well-known method, i.e. Fourier analysis. It is important for the system to work in the desired way by performing these analyses. When evaluated in terms of electrical machines, harmonics cause heating in magnetic components [45], voltage distortions in generators, and heat production and acoustic noise in motors [46]. In general, harmonics in electrical machines are exposed to the form of heat and cause losses in the machine [47].

When periodic functions are expressed in the Fourier series, the first term can be written as a constant and the other terms as a series of cosines and sines of the floors of a variable. Using the graphical method, the harmonic spectrum of non-sinusoidal waves can be determined from Fourier equations. In this method, the wave is divided into equidistant vertical parts and the average value of each part is determined [48]. The Fourier coefficients are expressed in Equations (5) and (6):

$$A_n = \frac{2}{m}\sum_{k=1}^{m} (y_k \times \sin(n \times \theta_k)) \tag{5}$$

Downloaded from https://academic.oup.com/ce/article/7/5/1058/7283059 by ANKOS Consortium (UK - ANB Free Trial Account) user on 13 November 2023

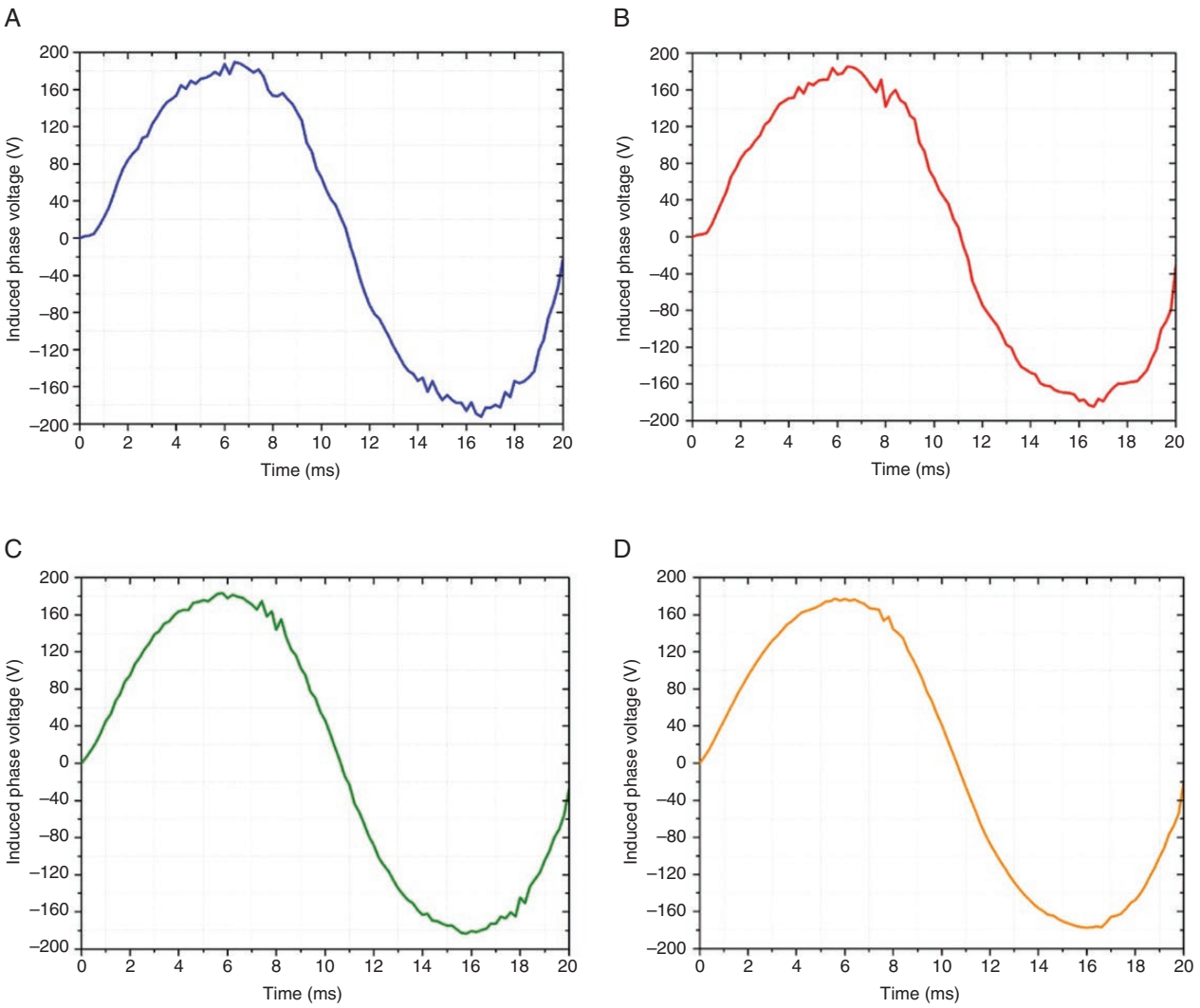



**Fig. 7:** Phase voltage waveforms of (a) Design 1, (b) Design 2, (c) Design 3 and (d) Design 4, respectively, at ω = 428.5 rpm.

**Table 3:** THD values of the designs

| Generator | THD (%) |
|---|---|
| Design 1 | 2.898 |
| Design 2 | 3.554 |
| Design 3 | 1.633 |
| Design 4 | 1.853 |

$$B_n = \frac{2}{m}\sum_{k=1}^{m}\left(y_k \times \cos\left(n \times \theta_k\right)\right) \tag{6}$$

where $m$ denotes the vertical division number of a non-sinusoidal wave, $\theta_k$ denotes the mean value of the divided parts on the $x$-axis ($k = 1, 2, \ldots, m$), $y_k$ defines the values of voltage and current corresponding to $\theta_k$ and $n$ defines the harmonic order [49]. The voltage can be expressed as in Equation (7) since it consists of the basic component and harmonic components [46]:

$$V_s(t) = V_{s1}(t) + \sum_{h>1} V_{sh}(t) \tag{7}$$

where $V_{s1}(t)$ denotes the main component and $V_{sh}(t)$ represents the harmonic component. The waveforms of the phase voltages obtained from the designed generators are given in Fig. 7.

The function of the voltage amplitude can be expressed in terms of Equations (5) and (6) as follows using the Fourier coefficients [47, 48]:

$$V(\theta) = \left(\sqrt{A_1^2 + B_1^2}\right)\sin\left[\theta + \tan^{-1}\left(\frac{B_1}{A_1}\right)\right] + \ldots + \left(\sqrt{A_n^2 + B_n^2}\right)\sin\left[\theta + \tan^{-1}\left(\frac{B_n}{A_n}\right)\right] \tag{8}$$

The distortions in the current or voltage waveforms are expressed in % by using the THD correlation. The voltage distortion components in Equation (8) are put into Equation (9) and the THD of the corresponding voltage is obtained:

$$V_{dis}(t) = V_s(t) - V_{s1}(t)\sum_{h=1} V_{sh}(t) \tag{9}$$

and

$$\%THD = 100 \times \frac{V_{dis}}{V_{s1}} \tag{10}$$

Table 3 contains the %THD values.

In the study, a harmonic spectrum was extracted for each design with the help of MATLAB® software (licence number: 40692431) following the use of the main and harmonic components, whose amplitudes and angles are presented in Table 3.

Taking Table 3 and Fig. 8 together, Design 2 has a relatively higher THD value than the other designs. As seen in Fig. 8, especially the fifth and seventh harmonics are higher in amplitude.

Downloaded from https://academic.oup.com/ce/article/7/5/1058/7283059 by ANKOS Consortium (UK - ANB Free Trial Account) user on 13 November 2023

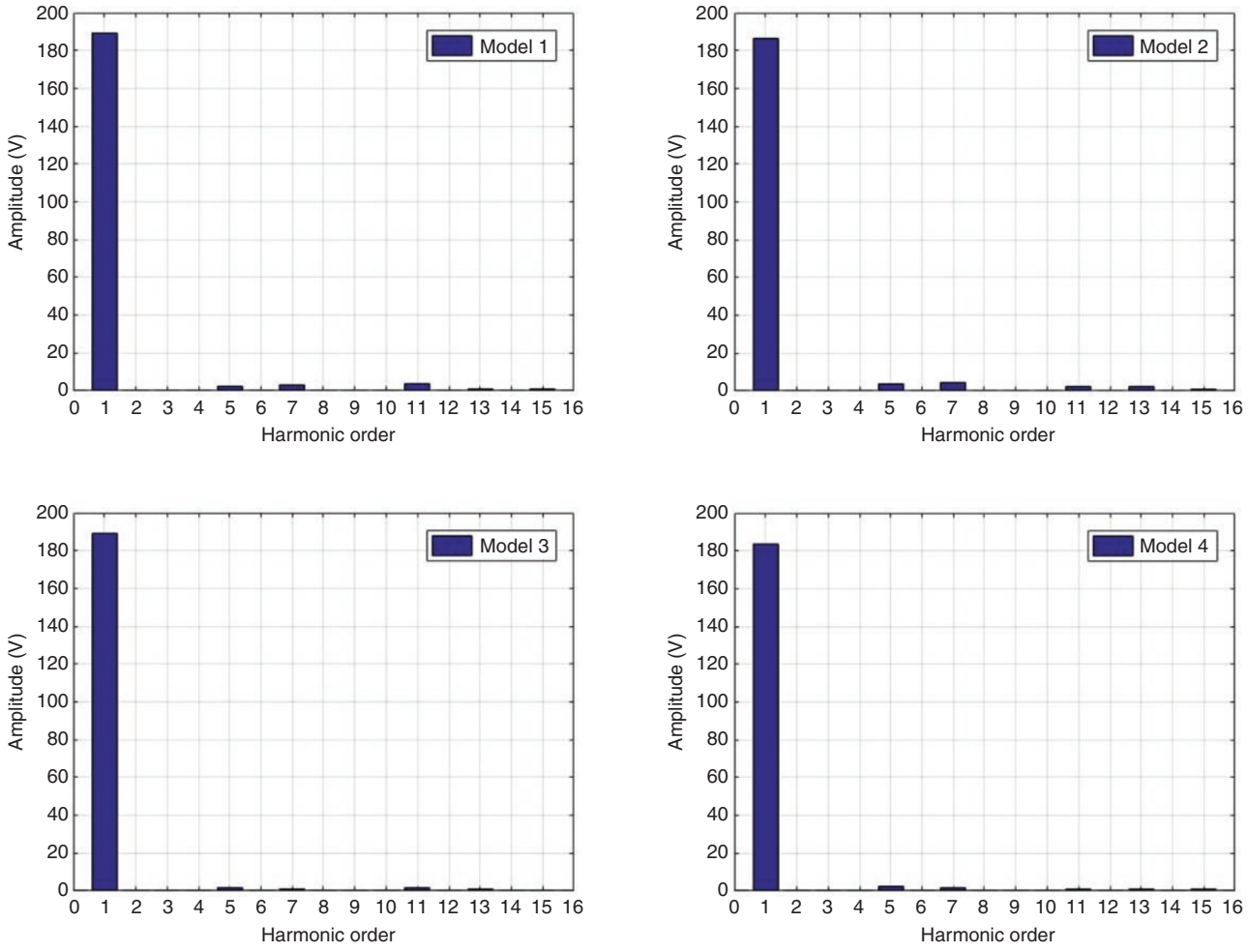



**Fig. 8:** Harmonic spectra of the designs.

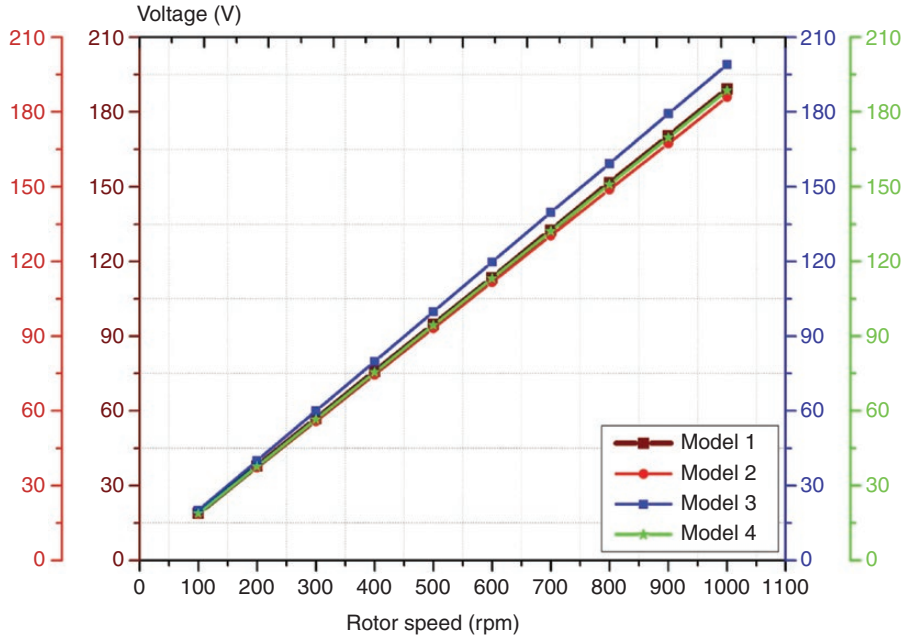



**Fig. 9:** RMS voltage versus rotor speed for the no-load case.

Downloaded from https://academic.oup.com/ce/article/7/5/1058/7283059 by ANKOS Consortium (UK - ANB Free Trial Account) user on 13 November 2023

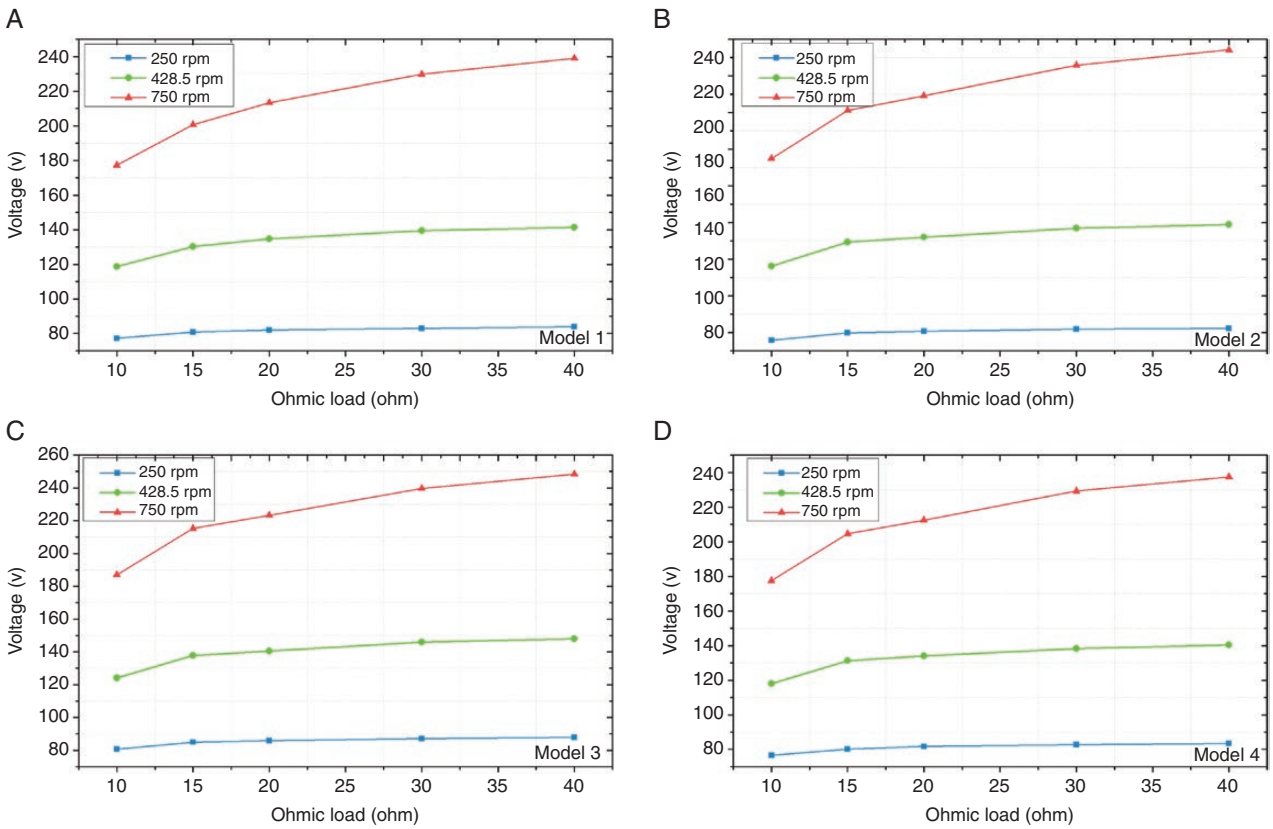



**Fig. 10:** The RMS voltage versus ohmic load for various rotor speeds. (a) Design 1, (b) Design 2, (c) Design 3 and (d) Design 4.

## 2.4 Simulation of voltage generation

The magnetodynamic analyses of four designs are presented for no-load and various resistive loads between $R = 10$ and 40 Ω under various rated speeds, namely 250, 428.5 and 750 rpm. Fig. 9 shows the root mean square (RMS) voltage values of a single phase for four designs for the no-load case. An overall appearance proves that Design 3 had the highest voltage value among the four designs, followed by Designs 1, 4 and 2, respectively, from high to low voltage. It is remarkable that a linear dependence on the rotor speed is preserved for all designs in the no-load case.

For example, Designs 1, 2, 3 and 4 generated the RMS phase voltage values of $V_{rms}$ = 189.17, 186.05, 199.02 and 188.57 V, respectively. Since the output load affects the power consumption of the machine, we have explored the characteristics of designs under different resistive loads. Fig. 10a–d shows the voltage plots under various operating speeds. As also proved in the previous figure (i.e. Fig. 9), the output voltage increases drastically at the rotation speed for all designs.

The generated voltage has increasing trends with a slightly decreasing slope due to optimal power conditions. It is known that the optimal power is taken from the machine for the same internal impedance value of the load. This situation manifests itself with decreasing slopes in all plots. Among the mentioned resistive loads, a value of 30 Ω gives the optimum power point in this respect. The maximum voltage is obtained for 1000 rpm and 40 Ω. Another important point is that the voltage slope increases more at low rotor speeds, as shown in Fig. 10a–d.

Upon evaluating all analyses together, it is observed that generators have similar flux distributions in terms of magnetic flux distributions. Considering the *B–H* characteristic curve of the core material M19 steel used, all geometries are outside the saturation in each generator. The variation of the no-load phase voltages with respect to the rotor speed is generally similar. Designs 3 and 4 have values relatively higher than those of the other designs.

When evaluated in terms of CT, which is an important problem with PM machines, a 60% improvement is achieved in Design 3 and 80% in Design 4 compared with the initial design. In terms of THD, another important criterion for generators, the performance of Design 4 is obtained as the best.

## 3 Conclusions

The negative environmental impact of fossil resources and the limited availability of reserves bring alternative energy sources to the agenda. Renewable energy sources are a significant alternative in terms of energy diversification and supply security. Wind energy, a renewable resource, is a clean and environmentally friendly resource. Generators are among the most important components of wind energy systems. Therefore, the performance of the generator is critical for the efficiency of the total system. PMSGs provide high power density, high torque density and high efficiency. In power generation, the THD value of the generated voltage and the CT in magnet machines are important design parameters.

The structure and material of the magnet in the generator impact the performance of the machine. In the study, the effects of different magnet structures on magnetic flux density distribution, CT, generated voltage and efficiency were investigated. Furthermore, to obtain detailed performance of generators, the voltages generated at different speeds and loads were investigated. The generated voltage had increasing trends with a slightly decreasing slope due to optimal power conditions. Considering

Downloaded from https://academic.oup.com/ce/article/7/5/1058/7283059 by ANKOS Consortium (UK - ANB Free Trial Account) user on 13 November 2023

the total harmonic distortions, it was realized that the best design was Design 3 with 1.633% THD. When the performance of this design was analysed, it was observed to have the lowest CT among the proposed models with a torque of 159.60 mNm. The generator with the lowest CT (89.95 mNm) was found to have a THD of 1.853%. However, it provided a 69-W decrease in the output power of this machine compared with the original design (i.e. Design 1). As an undesirable situation in PM machines, the CT and the THD values are expected to be as low as possible.

Taking into account all the above-mentioned information, Designs 3 and 4 were revealed to be the most suitable. Thus, Design 4 provided an 80% improvement in CT compared with the conventional machine type. It would appear that Design 4 exhibited the best performance among all the designs. Therefore, this technique can be used for other machines to obtain better CT and THD values. The voltage trends over the loads were similar. However, Design 3 produced the highest output among all the designs.

In the future, researchers can focus on the performance of generators under unbalanced load, their overload performance and the achievement of the partial demagnetization state in future studies.

## Funding

This research did not receive any specific grant from funding agencies in the public, commercial, or not-for-profit sectors.

## Conflict of interest statement

The author(s) declare no potential conflicts of interest with respect to the research, authorship and/or publication of this article.

## Data Availability

The data underlying this article are available in the article.

## References

[1] Pareek A, Dom R, Gupta J, Chandran JV, *et al*. Insights into renewable hydrogen energy: recent advances and prospects. *Mater Sci Energy Technol*, 2020, 3:319–327.

[2] IEA. *World Energy Outlook 2014*. Paris, France: International Energy Agency.

[3] Mutlu B, Kurt E, Bizon N, *et al*. Design and fabrication of a new micro-power scaled electromagnetic harvester. *J Energy Syst*, 2019, 3:51–66.

[4] Bouloukza I, Mordjaoui M, Kurt E, *et al*. Electromagnetic design of new radial flux permanent magnet motor. *J Energy Syst*, 2018, 2:13–27.

[5] Mughess N, Jaffery MH, Mughess A, *et al*. Reinforcement learning-based composite differential evolution for integrated demand response scheme in industrial microgrids. *Appl Energy*, 2023, 342:121150.

[6] Mughess N, Jaffery MH, Mughess A, *et al*. Bi-LSTM-based deep stacked sequence-to-sequence autoencoder for forecasting solar irradiation and wind speed. *Computers, Materials & Continua*, 2023, 75:6375–6393.

[7] Polinder H, Van der Pijl FFA, de Vilder GJ, *et al*. Comparison of direct-drive and geared generator concepts for wind turbines. *IEEE Trans Energy Convers*, 2006, 1:725–733.

[8] Özdemir MS, Ocak C, Dalcalı A. Permanent magnet wind generators: neodymium vs. ferrite magnets. In: *3rd International Congress on Human-Computer Interaction, Optimization and Robotic Applications*, Ankara, Turkey, 11–13 June 2021, 1–6.

[9] Touati Z, Pereira M, Araújo RE, *et al*. Integration of switched reluctance generator in a wind energy conversion system: an overview of the state of the art and challenges. *Energies*, 2022, 15:4743.

[10] Xing C, Jibin H, Kai C, *et al*. Modeling of electromagnetic torque considering saturation and magnetic field harmonics in permanent magnet synchronous motor for HEV. *Simul Model Pract Theory*, 2016, 66:212–225.

[11] Ma Q, El-Refaie A, Lequesne B. Low-cost interior permanent magnet machine with multiple magnet types. *IEEE Trans IA*, 2020, 56:1452–1463.

[12] Mughees N, Jaffery MH, Jawad M. A new predictive control strategy for improving operating performance of a permanent magnet synchronous generator-based wind energy and superconducting magnetic energy storage hybrid system integrated with grid. *J Energy Storage*, 2022, 55:105515.

[13] Junejo AR, Gilal NU, Doh J. Physics-informed optimization of robust control system to enhance power efficiency of renewable energy: application to wind turbine. *Energy*, 2023, 263:125667.

[14] Wang H, Qu Z, Tang S, *et al*. Analysis and optimization of hybrid excitation permanent magnet synchronous generator for stand-alone power system. *J Magn Magn Mater*, 2017, 436:117–125.

[15] Zala BO, Pugachov V. Methods to reduce cogging torque of permanent magnet synchronous generator used in wind power plants. *Elektron Elektrotech* , 2017, 23:43–48.

[16] Lee JH, Lee HK, Lee YG, *et al*. Design and analysis considering magnet usage of permanent magnet synchronous generator using analytical method. *Electronics*, 2022, 11:205.

[17] Jia L, Lin M, Le W, *et al*. Dual-skew magnet for cogging torque minimization of axial flux PMSM with segmented stator. *IEEE Trans Magn*, 2020, 56:7507306.

[18] Dajaku G, Gerling D. PM wind generator with reduced amount of rare-earth magnet material. In: *International Conference on Clean Electrical Power*, Otranto, Italy, 2–4 July 2019, 15–21.

[19] Habib A, Che HS, Rahim NA, *et al*. A fully coreless multi-stator multi-rotor (MSMR) AFPM generator with combination of conventional and Halbach magnet arrays. *Alexandria Eng J*, 2020, 59:589–600.

[20] Fang H, Song R, Cai X. Analysis and reduction of cogging torque for magnetic-gear PMSG used in wave energy conversion. In: *22nd International Conference on Electrical Machines and Systems*, Harbin, China, 11–14 August 2019.

[21] Anuja TA, Doss MAN. Asymmetrical magnets in rotor structure of a permanent magnet brushless DC motor for cogging torque minimization. *J Electr Eng Technol*, 2022, 17:1271–1279.

[22] Zakir MR, Ikram J, Shah SI, *et al*. Performance improvement of axial flux permanent magnet machine with phase group concentrated coil winding. *Energies*, 2022, 15:7337.

[23] Özmen T, Onat N. The effects of magnetic circuit geometry and material properties on surface mounted permanent magnet synchronous generator performance. *Balkan Journal of Electrical and Computer Engineering*, 2021, 9:99–105.

[24] Kim DH, Kim KS, Yang IJ, *et al*. Alternative bridge spoke permanent magnet synchronous generator design for wind power generation systems. *IEEE Access*, 2021, 9:152819–152828.

[25] Santiago JAE, Danguillecourt OL, Duharte GI, *et al*. Dimensioning optimization of the permanent magnet synchronous generator for direct drive wind turbines. *Energies*, 2021, 14:7106.

Downloaded from https://academic.oup.com/ce/article/7/5/1058/7283059 by ANKOS Consortium (UK - ANB Free Trial Account) user on 13 November 2023

[26] Amin S, Madanzadeh S, Khan S, *et al*. Effect of the magnet shape on the performance of coreless axial flux permanent magnet synchronous generator. *Electr Eng*, 2022, 104:959–968.
[27] Baig MA, Ikram J, Iftikhar A, *et al*. Minimization of cogging torque in axial field flux switching machine using arc shaped triangular magnets. *IEEE Access*, 2020, 8:227193–227201.
[28] Nazir M, Ikram J, Yousuf M, *et al*. Investigation of sinusoidal shaped rotor to reduce torque ripple in axial flux permanent magnet machine. *Int J Ambient Energy*, 2022, 43:8113–8122.
[29] Mahmood Z, Ikram J, Badar R, *et al*. Minimization of torque ripples in multi-stack slotted stator axial-flux synchronous machine by modifying magnet shape. *Mathematics*, 2022, 10:1653.
[30] Brescia E, Palmieri M, Massenio PR, *et al*. Cogging torque suppression of modular permanent magnet machines using a semi-analytical approach and artificial intelligence. *IEEE Access*, 2023, 11:39405–39417.
[31] Bień A, Drabek T, Kara D, *et al*. Reduction in the cogging torques in the DCEFSM motor by changing the geometry of the rotor teeth. *Energies*, 2022, 15:2455.
[32] Caruso M, Di Tommaso AO, Miceli R, *et al*. A cogging torque minimization procedure for interior permanent magnet synchronous motors based on a progressive modification of the rotor lamination geometry. *Energies*, 2022, 15:4956.
[33] Guanghui D, Niumei L, Qixun Z, *et al*. Multi-physics comparison of surface-mounted and interior permanent magnet synchronous motor for high-speed applications. *Machines*, 2022, 10:700.
[34] Gul W, Gao Q, Lenwari W. Optimal design of a 5-MW double-stator single-rotor PMSG for offshore direct drive wind turbines. *IEEE Trans IA*, 2020, 56:216–225.
[35] Zhang Z, Zhao Y, Qiao W, *et al*. Discrete-time direct torque control for direct-drive PMSG-based wind energy conversion systems. *IEEE Trans IA*, 2015, 51:3504–3514.
[36] Zeng X, Liu T, Wang S, *et al*. Comprehensive coordinated control strategy of PMSG-based wind turbine for providing frequency regulation services. *IEEE Access*, 6394, 2019:4–63953.
[37] Dalcalı A, Kurt E, Çelik E, *et al*. Cogging torque minimization using skewed and separated magnet geometries. *J Polytechnic*, 2020, 23:223–230.
[38] Dalcalı A. Influence of rotor magnet material and stator winding geometry on output torque in spherical actuator. *J Eng Sciences Des*, 2019, 7:145–151.
[39] He Y, Yu C, Haidar S, *et al*. High-performance on-chip hot-pressed NdFeB hard magnets for MEMS applications. *IEEE Trans Magnetics*, 2021, 57:2101504.
[40] Yang Y, Ren R, Wang Y, *et al*. Effect of molding pressure on structure and properties of ring-shaped bonded NdFeB magnet. *IEEE Trans Magnetics*, 2020, 56:1000105.
[41] Omran HRG, Gholamian SA, Hashemnia MN, *et al*. Design optimization of a five-phase IPM synchronous motor for low-speed applications. *Iran J Sci Technol Trans Electr Eng*, 2016, 40:79–91.
[42] Zhao W, Lipo TA, Kwon BI. Torque pulsation minimization in spoke-type interior permanent magnet motors with skewing and sinusoidal permanent magnet configurations. *IEEE Trans Magnetics*, 2015, 51:81108041–81108044.
[43] Sun S, Jiang F, Li T, *et al*. Design and optimization of a novel axial-radial flux permanent magnet machine. *IEEE Trans Appl Superconductivity*, 2020, 30:5205106.
[44] Dosiek L, Pillay P. Cogging torque reduction in permanent magnet machines. *IEEE Trans Ind Appl*, 2007, 43:1565–1571.
[45] Ingale R. Harmonic analysis using FFT and STFT. *International J Signal Process, Image Process and Pattern Recognit*, 2014, 7:345–362.
[46] Lo WC, Chan CC, Zhu ZQ, *et al*. Acoustic noise radiated by PWM-controlled induction machine drives. *IEEE Trans I Electronics*, 2000, 47:880–889.
[47] Ocak C, Dalcalı A. A comparative analysis of four-pole brushless DC motors with different slot and winding arrangement based on THD values. *International J Energy Applications and Technologies*, 2020, 7:7–12.
[48] Kocatepe C, Uzunoğlu M, Yumurtacı R, *et al*. *Harmonics in Electric Plants*. Istanbul, Turkey: Birsen Publishing House, 2003 (in Turkish).
[49] Mohan N, Undeland TM, Robbins VP. *Power Electronics: Converters, Applications, and Design*. Hoboken, NJ, USA: John Wiley & Sons, 2003.

Downloaded from https://academic.oup.com/ce/article/7/5/1058/7283059 by ANKOS Consortium (UK - ANB Free Trial Account) user on 13 November 2023